Journal of Controlled Release 244 (2016) 326–335

Contents lists available at ScienceDirect

Journal of Controlled Release

journal homepage: www.elsevier.com/locate/jconrel

Self-crosslinkable and intracellularly decrosslinkable biodegradable micellar nanoparticles: A robust, simple and multifunctional nanoplatform for high-efficiency targeted cancer chemotherapy

Yan Zou, Ya Fang, Hao Meng, Fenghua Meng *, Chao Deng, Jian Zhang, Zhiyuan Zhong *

[a] Biomedical Polymers Laboratory, College of Chemistry, Chemical Engineering and Materials Science, Soochow University, Suzhou, 215123, PR China
[b] Jiangsu Key Laboratory of Advanced Functional Polymer Design and Application, College of Chemistry, Chemical Engineering and Materials Science, Soochow University, Suzhou, 215123, PR China

ARTICLE INFO

Article history:
Received 18 April 2016
Received in revised form 23 May 2016
Accepted 27 May 2016
Available online 28 May 2016

Keywords:
Targeted delivery
RGD peptide
Bioresponsive
Biodegradable micellar nanoparticles
Disulfide
Melanoma

ABSTRACT

Nanomedicines based on biodegradable micelles offer a most promising treatment for malignant tumors. Their clinical effectiveness, however, remains to be improved. Here, we report that self-crosslinkable and intracellularly decrosslinkable micellar nanoparticles (SCID-Ms) self-assembled from novel amphiphilic biodegradable poly(ethylene glycol)-*b*-poly(dithiolane trimethylene carbonate) block copolymer achieve high-efficiency targeted cancer chemotherapy *in vivo*. Interestingly, doxorubicin (DOX)-loaded SCID-Ms showed favorable features of superb stability, minimal drug leakage, long circulation time, triggered drug release inside the tumor cells, and an unprecedented maximum-tolerated dose (MTD) of over 100 mg DOX equiv./kg in mice, which was at least 10 times higher than free drug. The *in vivo* studies in malignant B16 melanoma-bearing C57BL/6 mice revealed that DOX-SCID-Ms at a dosage of 30 mg DOX equiv./kg could effectively suppress tumor growth and prolong mice survival time without causing obvious systemic toxicity. Moreover, DOX-SCID-Ms could be readily decorated with a targeting ligand like cRGD peptide. The biodistribution studies showed that cRGD20/DOX-SCID-Ms had a high tumor accumulation of 6.13% ID/g at 6 h post injection, which was *ca.* 3-fold higher than that for clinically used pegylated liposomal doxorubicin (DOX-LPs). Accordingly, cRGD20/DOX-SCID-Ms exhibited significantly better therapeutic efficacy and lower side effects than DOX-LPs in B16 melanoma-bearing mice. These self-regulating biodegradable micellar nanoparticles offer a robust, multifunctional and viable nanoplatform for targeted cancer chemotherapy.

1. Introduction

Nanomedicines based on biodegradable micelles and nanoparticles offer a most promising treatment for malignant tumors [1–4]. Their clinical effectiveness, however, remains to be further improved by increasing their systemic stability, tumor accumulation and selectivity, and/or control over drug release [5–8]. In the past years, various stimuli-responsive multifunctional nanosystems have been developed to achieve enhanced therapeutic efficacy in different tumor models [9–13]. The typically sophisticated design and fabrication, potential safety and toxicity concerns, and high cost, however, preclude their clinical translation [14–17]. Lack of safe, simple and therapeutically effective nanovehicles has been a long challenge for the clinical translation of anticancer nanomedicines [18–22].

In this study, we have designed and developed self-crosslinkable and intracellularly decrosslinkable micellar nanoparticles (SCID-Ms) for high-efficiency targeted cancer chemotherapy *in vivo* (Scheme 1). SCID-Ms are self-assembled from novel amphiphilic biodegradable poly(ethylene glycol)-*b*-poly(dithiolane trimethylene carbonate) (PEG-*b*-PDTC) block copolymer, in which the hydrophobic PDTC block is composed of biodegradable poly(trimethylene carbonate) (PTMC) main chain and multiple dithiolane rings at the side. PTMC and its derivatives with excellent biocompatibility and biodegradability have been widely used for various biomedical applications such as absorbable sutures, tissue engineering, and drug and gene delivery [23–28]. The pendant dithiolane ring is analogous to that of the lipoic acid, a natural antioxidant produced by the human body and a drug used for Alzheimer's disease and diabetes [29]. Notably, dextran–lipoic acid and hyaluronic acid–lysine–lipoic acid conjugates furnished, in the presence of a catalytic amount of dithiothreitol, reduction-sensitive reversibly crosslinked nanoparticles [30–31]. The past years have witnessed a remarkable development of reduction-sensitive nanoparticles for triggered cytoplasmic drug and gene delivery [32–41], based on the fact that there exists 2–3 orders magnitude higher redox potential in the cytoplasm of tumor cells than in the blood circulation [42–43]. Intriguingly, these novel self-crosslinkable bioresponsive biodegradable micellar nanoparticles are not only multifunctional but also simple and easy to prepare, which makes them unique and particularly promising for translational research.

* Corresponding authors.
E-mail addresses: fhmeng@suda.edu.cn (F. Meng), zyzhong@suda.edu.cn (Z. Zhong).

http://dx.doi.org/10.1016/j.jconrel.2016.05.060
0168-3659/

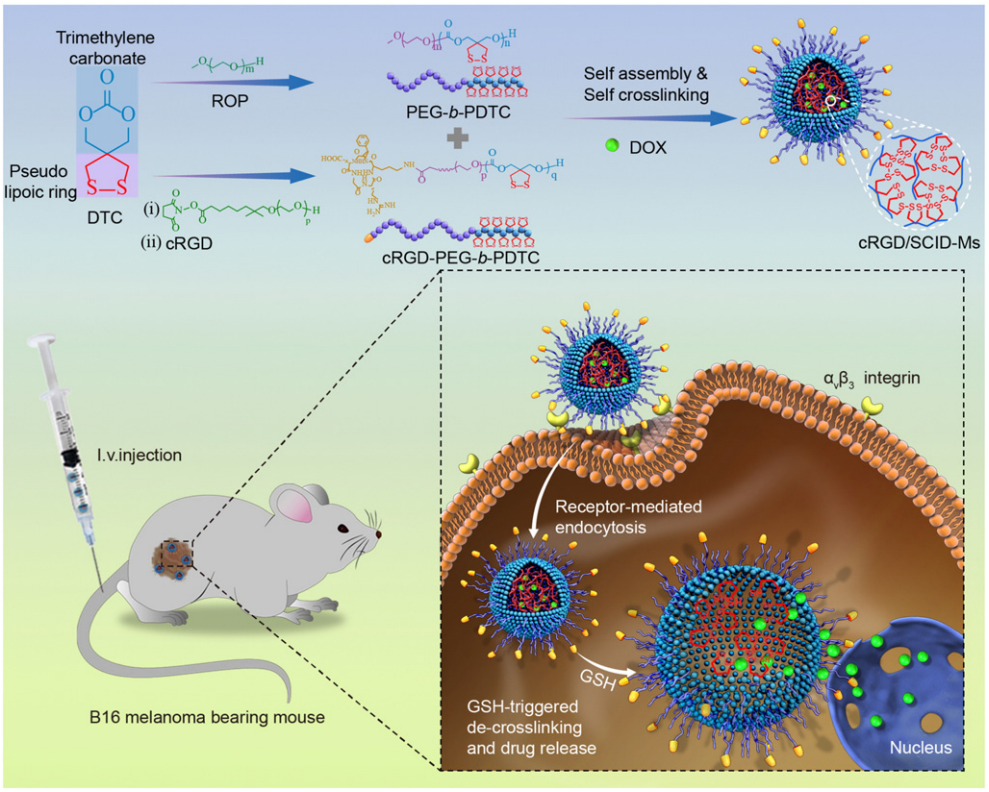

Scheme 1. Schematic diagram depicting formation and *in vivo* tumor-targeting doxorubicin delivery of cRGD-decorated self-crosslinkable and intracellularly decrosslinkable micellar nanoparticles (cRGD/SCID-Ms).

2. Materials and methods

2.1. Materials

Methoxy poly(ethylene glycol) (MeO-PEG-OH, M_n = 5.0 kg/mol, PDI = 1.03, Fluka) and *N*-hydroxysuccinimide activated poly(ethylene glycol) (NHS-PEG-OH, M_n = 6.5 kg/mol, PDI = 1.04, Suzhou Nord Derivatives Pharm-tech Co. Ltd) were dried by azeotropic distillation from anhydrous toluene. Dichloromethane (DCM) was dried by refluxing over CaH_2 and distilled prior to use. Zinc bis [bis(trimethylsilyl) amide] (97%, Aldrich), C(RGDfK) (cRGD, 98%, China Peptides Co., Ltd.), glutathione (GSH, 99%, Roche), and doxorubicin hydrochloride (DOX·HCl, >99%, Beijing Zhongshuo Pharmaceutical Technology Development) were used as received.

2.2. Characterization

The polymer structures were characterized using ^{1}H NMR on a Unity Inova 400 spectrometer operating at 400 MHz. The chemical shifts were calibrated against residual solvent signal. The molecular weight and polydispersity of copolymers were determined by a Waters 1515 gel permeation chromatograph (GPC) instrument equipped with two linear PLgel columns (500 Å and Mixed-C) following a guard column and a differential refractive-index detector. The measurements were performed using DMF as an eluent at a flow rate of 1.0 mL/min at 30 °C and a series of narrow polystyrene standards for the calibration of the columns. The size and size distribution of micellar nanoparticles were determined at 25 °C using dynamic light scattering (DLS, Zetasizer Nano-ZS, Malvern Instruments) equipped with a 633 nm He–Ne laser using back-scattering detection. Zeta potential measurements were carried out using a Zetasizer Nano-ZS instrument (Malvern) equipped with a standard capillary electrophoresis cell. The measurements were performed in triplicate. Transmission electron microscopy (TEM) was performed using a Tecnai G220 TEM operated at an accelerating voltage of 120 kV. The samples were prepared by dropping 10 μL of 0.2 mg/mL micellar nanoparticle suspension on the copper grid followed by staining with phosphotungstic acid (1 wt.%). The CLSM images were taken on a confocal laser scanning microscope (TCS SP5). The absorbance of dithiolane rings in the micellar nanoparticles at 330 nm was monitored using a double-beam UV–visible system (UH5300 Hitachi). PEG-PCL micellar nanoparticle dispersions were used for calibration.

2.3. Synthesis of dithiolane-functionalized cyclic trimethylene carbonate (DTC)

DTC was synthesized in two steps (Scheme 2). Firstly, to a solution of 2,2-bis (bromomethyl)-1,3-propanediol (20 g, 0.08 mol) in DMF (350 mL) under stirring was added NaSH·H_2O (28.26 g, 0.38 mol). The reaction was allowed to proceed at 75 °C for 48 h under constant stirring. The solvent was removed by distillation under reduced pressure. The residue was diluted with D.I. water (300 mL) and extracted with EtOAc (3 × 250 mL). The organic phase was dried over anhydrous $MgSO_4$. The solvent was evaporated to yield 2-(1,2-dithiolan-4-yl)-1,3-

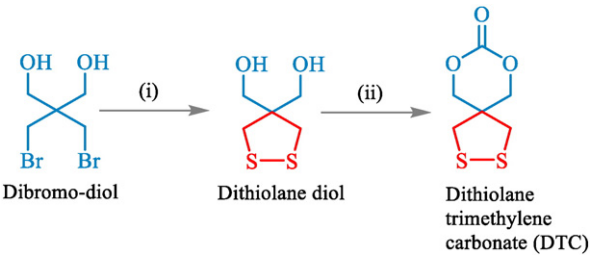

Scheme 2. Synthesis of dithiolane-functionalized cyclic carbonate (DTC). Conditions: (i) NaSH, DMF, 75 °C, 48 h, and in air for 24 h; (ii) ethyl chloroformate, Et_3N, THF, 0 °C, 4 h.

diol as a yellowish oil. Yield: 8.7 g (67.8%). ^{1}H NMR (400 MHz, $CDCl_3$): δ 3.64 (s, 4H, —C(C$\underline{H_2}$OH)$_2$), 2.67 (s, 4H, —$\underline{CH_2}$S S$\underline{CH_2}$—).

To 200 mL dry THF solution of 2-(1,2-dithiolan-4-yl)-1,3-diol (8.7 g, 51.8 mmol) and ethyl chloroformate (11.9 g, 108.8 mmol) was dropwise added a solution of Et_3N (15.3 mL, 51.1 mmol) in THF (5 mL) at 0 °C under stirring. The reaction was allowed to proceed for 4 h at 0 °C. The reaction mixture was filtered, and the filtrate was dried under reduced pressure. The final product, dithiolane-functionalized cyclic carbonate (DTC), was obtained by re-crystallization twice from THF. Yield: 6.3 g (67.3%). ^{1}H NMR (400 MHz, $CDCl_3$): δ 4.46 (s, 4H, —COO($\underline{CH_2}O$)$_2$C—), 3.13 (s, 4H, —$\underline{CH_2}$SS$\underline{CH_2}$—). ^{13}C NMR (400 MHz, DMSO-d_6): δ 147.23 (—$\underline{C}$OO(CH$_2$$\underline{O}$)$_2$C—), 74.54 (—COO($\underline{CH_2}O$)$_2$C—), 42.84 (—COO(CH$_2$$\underline{O}$)$_2$$\underline{C}$—), and 28.95 (—$\underline{CH_2}SS\underline{CH_2}$—). Elemental analysis for DTC ($C_5H_8O_3S_2$): C; 41.64%, H: 4.17%. Found: C: 41.80%, H: 4.20%. TOF-MS (*m*/*z*) for $C_5H_8O_3S_2$: calculated 192.0 Da, found 192.3 Da.

2.4. Synthesis of PEG-*b*-PDTC block copolymer via ring-opening polymerization

Typically, under a nitrogen atmosphere, into a stirred solution of PEG (M_n = 5.0 kg/mol, 0.2 g, 0.04 mmol) and DTC (0.2 g, 1.04 mmol) in anhydrous CH_2Cl_2 (3 mL) was quickly added 0.5 mL of zinc bis [bis(trimethylsilyl) amide] stock solution (40 mM) in CH_2Cl_2 (Scheme 3). The reaction vessel was sealed and placed in an oil-bath thermostated at 40 °C. After 24 h, the reaction was terminated by adding acetic acid. A sample was taken for the determination of monomer conversion using ^{1}H NMR. The PEG-*b*-PDTC copolymer was isolated by precipitation in cold ethyl ether, filtration and drying under vacuum for 2 days. Yield: 81%. ^{1}H NMR (400 MHz, $CDCl_3$): δ 4.35 (s, 4H, —CO$\underline{CH_2}$—), 3.65 (s, 4H, —$\underline{CH_2CH_2}$O—), 3.37 (s, $\underline{CH_3}$O—), 3.04 (s, —C(CH$_2$S S$\underline{CH_2}$)—), M_n (^{1}H NMR) = 8.9 kg/mol. M_n (GPC) = 11.2 kg/mol. PDI = 1.51.

2.5. Colloidal stability and reduction responsivity of SCID-Ms

Micellar nanoparticles were prepared by a solvent exchange method. Typically, 1.8 mL of phosphate buffer (PB, 10 mM, pH 7.4) was dropwise added to 0.2 mL of copolymer solution in DMF (2.0 mg/mL) at r.t. under constant stirring. Micellar nanoparticles were obtained by dialysis against the same PB for 12 h (Spectra/Pore, MWCO 3500). The micellar nanoparticles were self-crosslinked when placed at 37 °C for 24 h. The colloidal stability of crosslinked micellar nanoparticles against extensive dilution, 10% FBS, or 10 mM GSH was investigated using DLS.

2.6. Preparation of DOX-SCID-Ms

Desalted DOX was used as a model hydrophobic anticancer drug. DOX was obtained by desalting DOX·HCl using triethylamine in DMSO. DOX-SCID-Ms were prepared using the above procedure for SCID-Ms except that a copolymer solution containing different amounts of DOX (at 9.1 or 16.7 wt.% feed ratio) was used and stirred for 0.5 h before dialysis. The amount of DOX was determined using fluorescence measurement (excitation at 480 nm). For determination of drug loading content, DOX-SCID-Ms were lyophilized and dissolved in DMF and analyzed with fluorescence spectroscopy, wherein calibration curve was obtained with DOX/DMF solutions with different DOX concentrations. Drug loading content (DLC) and drug loading efficiency (DLE) were calculated according to the following formula:

$$\text{DLC (wt.\%)} = \text{weight of loaded drug/total weight of polymer and loaded drug)} \times 100$$

$$\text{DLE (\%)} = (\text{weight of loaded drug/weight of drug in feed}) \times 100$$

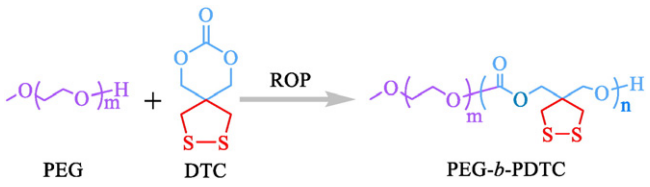

Scheme 3. Synthesis of PEG-*b*-PDTC block copolymer by ring-opening copolymerization of DTC using methoxyl PEG (M_n = 5.0 kg/mol) as an initiator and zinc bis [bis(trimethylsilyl) amide] as a catalyst in CH_2Cl_2 at 40 °C.

2.7. Triggered drug release of DOX-SCID-Ms

The *in vitro* release studies were conducted in a dialysis tube (Spectra/Por 12,000–14,000) at 37 °C with 0.5 mL of DOX-SCID-Ms (30 mg/L) dialysis against 25 mL of release media, *i.e.*, PB or PB containing 10 mM GSH. At desired time intervals, 5 mL of release media was taken out and replenished with an equal volume of fresh media. The amount of DOX released was determined using fluorometry. The release experiments were conducted in triplicates.

2.8. MTT assays of DOX-SCID-Ms

B16 mouse melanoma cells were plated in a 96-well plate (5×10^3 cells/well) in 100 μL of RPMI 1640 media containing 10% fetal bovine serum, 1% L-glutamine, and antibiotics penicillin (100 IU/mL) and streptomycin (100 μg/mL) for 24 h. The medium was aspirated and replaced by 90 μL of fresh medium and 10 μL DOX-SCID-Ms in PB (10 mM, pH 7.4) was added to yield final DOX concentrations ranging from 0.01 to 40 μg/mL. The cells were cultured for 48 h. 10 μL of 3-(4,5-dimethylthiazol-2-yl)-2,5-diphenyltetrazoliumbromide (MTT) solution (5 mg/mL) was added. The cells were cultured for another 4 h, the medium was aspirated, the MTT-formazan generated by live cells was dissolved in 150 μL of DMSO, and the absorbance at 492 nm of each well was measured using a microplate reader. The relative cell viability (%) was determined by comparing the absorbance at 492 nm with control wells containing only culture medium. Data are presented as average ± SD (n = 4). The cytotoxicity of blank SCID-Ms was assessed in a similar way.

2.9. Confocal microscopy of DOX-SCID-Ms

The cellular uptake and intracellular drug release behaviors of DOX-SCID-Ms were followed with confocal laser scanning microscopy (CLSM). B16 cells were cultured on microscope slides in a 24-well plate (5×10^4 cells/well) using RPMI-1640 medium for 24 h. The cells were incubated with DOX-SCID-Ms for 2 or 8 h before the culture medium was removed. The cell nuclei and skeleton were stained with 4′,6-diamidino-2-phenylindole (DAPI) and FITC-phalloidine, respectively. The fluorescence images were obtained using CLSM (TCS SP5).

2.10. Synthesis of cRGD-PEG-*b*-PDTC block copolymers

cRGD-PEG-*b*-PDTC diblock copolymer was synthesized *via* two steps. Firstly, NHS-PEG-*b*-PDTC was prepared as described above except NHS-PEG-OH (M_n = 6.5 kg/mol) was used as macro-initiator. Yield: 83.2%. ^{1}H NMR (400 MHz, $CDCl_3$): PEG: δ 3.64; DTC moieties: δ 4.32, 3.02, NHS moieties: δ 2.52. M_n (^{1}H NMR) = 10.2 kg/mol, M_n (GPC) = 13.2 kg/mol, PDI = 1.49. Secondly, cyclic peptide C(RGDfK) (cRGD) was conjugated to NHS-PEG-*b*-PDTC by amidation reaction. In brief, NHS-PEG-*b*-PDTC (0.2 g, 0.024 mmol) and cRGD (22 mg, 0.033 mmol) were added to 5 mL of DMF. The reaction proceeded for 24 h at r.t. The final product, cRGD-PEG-*b*-PDTC, was isolated through dialysis (MWCO 7000) against deionized water for 48 h followed by lyophilization. Yield: 82.7%. ^{1}H NMR (600 MHz, DMSO-d_6): PEG: δ 3.51; DTC: δ

4.13, 2.99; cRGD: δ 6.84–7.61. The degree of cRGD conjugation was determined to be 88% by a Micro BCA protein assay kit (Thermo Scientific).

2.11. MTT assays of cRGD/DOX-SCID-Ms

MTT assays were performed in $\alpha_v\beta_3$ overexpressing B16 melanoma cells. To evaluate the antitumor activity of cRGD/DOX-SCID-Ms, cells were incubated with cRGD/DOX-SCID-Ms or DOX-LPs (control) at DOX dosages ranging from 0.01 to 40 μg/mL in an atmosphere containing 5% CO_2 at 37 °C for 4 h. The medium was aspirated and replaced by fresh medium, the cells were cultured for another 44 h, 3-(4,5-dimethylthiazol-2-yl)-2,5-diphenyl tetrazoliumbromide (MTT) solution in PBS (10 μL, 5 mg/mL) was added, and the cells were cultured for another 4 h. The supernatant was carefully aspirated, the MTT-formazan generated by live cells was dissolved in 150 μL of DMSO, and the absorbance at 492 nm of each well was measured using a microplate reader. The absorbance of the control wells containing DMSO only was used as a background signal. The relative cell viability was determined by comparing the absorbance at 492 nm with cells cultured in RPMI-1640 medium (without exposure to micellar nanoparticles). The experiments were performed in quartets and data are presented as average ± SD ($n = 4$). The cytotoxicity of blank cRGD/SCID-Ms was assessed in a similar way.

2.12. Flow cytometry assays and confocal measurements of cRGD/DOX-SCID-Ms

B16 melanoma cells seeded in a 6-well plate (5×10^5 cells/well) were incubated with cRGD/DOX-SCID-Ms or DOX-LPs in 500 μL of PBS (DOX dosage = 10 μg/mL) at 37 °C for 4 h. The cells were digested by 0.25% (*w*/*v*) trypsin and 0.03% (*w*/*v*) EDTA. The suspensions were centrifuged at 1000 ×*g* for 3 min, washed twice with PBS, and then resuspended in 500 μL of PBS. Fluorescence histograms were immediately recorded with a BD FACS Calibur flow cytometer (Becton Dickinson, USA) and analyzed using Cell Quest software based on 10,000 gated events. The gate was arbitrarily set for the detection of FITC fluorescence.

B16 cells were cultured on microscope slides in 24-well plates (5×10^4 cells/well). The cells were incubated with DOX-SCID-Ms, cRGD20/DOX-SCID-Ms or DOX-LPs in 50 μL of PBS (DOX dosage = 10 μg/mL) at 37 °C. After 1 h incubation, the medium was aspirated and replaced by fresh medium, and the cells were further incubated for another 7 h. The culture medium was removed and the cells on microscope plates were washed three times with PBS before fixation with 4% paraformaldehyde solution for 15 min and three times wash with PBS. The cytoskeleton was stained with fluorescein isothiocyanate labeled phalloidin (phalloidin-FITC) for 1 h and washed with PBS for three times. The cell nuclei were stained with 4′,6-diamidino-2-phenylindole (DAPI) for 15 min and washed with PBS for three times. The fluorescence images were obtained using a confocal microscope (TCS SP5). For inhibition experiments, cells were pre-treated with 100 μg/mL free cRGD for 1 h before adding cRGD20/DOX-SCID-Ms.

2.13. Pharmacokinetics of DOX-SCID-Ms and cRGD20/DOX-SCID-Ms

All animal experiments were approved by the Animal Care and Use Committee of Soochow University (P.R. China), and all protocols of animal studies conformed to the Guide for the Care and Use of Laboratory Animals. For *in vivo* pharmacokinetic studies, C57BL/6 mice were intravenously injected with 200 μL of DOX-SCID-Ms or cRGD20/DOX-SCID-Ms, about 10 μL of blood was taken at different time points, and DOX was extracted by DMF solution (containing 50 mM HCl and 20 mM DTT) and determined by fluorescence measurement ($n = 5$). The blood circulation half-lives were obtained by second-order exponential decay fits.

2.14. In vivo biodistribution of DOX-SCID-Ms and cRGD20/DOX-SCID-Ms

B16 melanoma tumor models were generated by subcutaneous injection of 1×10^6 cells in 50 μL of PBS into the hind flank of the mice. The mice were used for treatment and biodistribution when the tumor volume reached 20–30 mm^3 and 100–150 mm^3, respectively. For *in vivo* biodistribution studies, C57BL/6 mice bearing B16 melanoma tumors were intravenously injected with 200 μL of DOX-SCID-Ms or cRGD/DOX-SCID-Ms. The mice were sacrificed at 6, 12 or 24 h post injection. The major organs were collected, flushed with PBS, wet weighed, homogenized and extracted by DMF solution (containing 50 mM HCl and 20 mM DTT). The DOX level was determined by fluorescence measurement ($n = 5$).

2.15. Therapeutic efficacy of DOX-SCID-Ms and cRGD20/DOX-SCID-Ms

For antitumor efficacy studies, C57BL/6 mice bearing B16 melanoma tumors were intravenously injected with 200 μL of DOX-SCID-Ms or cRGD20/DOX-SCID-Ms every two days *via* tail vein. The tumor size was measured every day using calipers. Mice were weighed every day and the relative body weight was normalized to their initial weight. On day 15, one mouse from each group was sacrificed by cervical vertebra dislocation and the heart, liver and kidney were isolated and prepared for histological analysis. For histological analyses, the tissues were fixed with 4% paraformaldehyde solution and embedded in paraffin. The sliced organ tissues (thickness: 4 mm) mounted on the glass slides were stained by hematoxylin and eosin (H&E) and observed by a digital microscope (Olympus BX41).

2.16. Maximum tolerated dose (MTD) studies

For MTD studies, C57BL/6 mice were administered with a single dose of DOX-SCID-Ms or cRGD20/DOX-SCID-Ms *via* tail vein injection. The body weight was monitored daily for 10 days. The MTD was defined as the highest dose that does not cause unacceptable toxicity like death, over 15% body weight loss or other remarkable changes in the general appearance of the mice within the experiment period.

3. Results and discussion

3.1. Synthesis of PEG-b-PDTC

To prepare PEG-*b*-PDTC diblock copolymer, we devised and synthesized a new monomer, dithiolane-functionalized cyclic carbonate (DTC), in two steps with a decent overall yield of 45.6% (Scheme 2). ^{1}H NMR showed two singlets at δ 3.13 and 4.46 attributable to the methylene protons in the dithiolane and next to the carbonate bond, respectively (Fig. 1a). Notably, the integral ratio of these two peaks was close to the theoretical value of 1:1. The structure of DTC was further verified by elemental analysis, electrospray ionization mass spectrometry and ^{13}C NMR (Fig. 1b). Ultraviolet (UV) spectrum of DTC showed characteristic absorbance of a dithiolane ring at 330 nm (Fig. 1c,d), analogous to lipoic acid [44]. The ring-opening polymerization of DTC using methoxy PEG ($M_n = 5.0$ kg/mol) as a macro-initiator at a monomer-to-initiator molar ratio of 26/1 and zinc bis [bis(trimethylsilyl) amide] as a catalyst yielded a PEG-*b*-PDTC diblock copolymer. ^{1}H NMR showed besides signals at δ 3.65 attributable to the methylene protons of the PEG block, resonances at δ 3.37 and 3.04 owing to the methylene protons of the PDTC block and a small peak at δ 4.35 assignable to the methylene protons of the PEG unit adjacent to the ester bond (Fig. 2). The comparison of the integrals of signals at δ 3.04 (methylene protons in dithiolane ring) to δ 3.65 revealed that the PDTC block had a degree of polymerization of about 20, corresponding to an M_n of 3.9 kg/mol. Gel permeation chromatography (GPC) curve showed a unimodal distribution with an M_w/M_n of 1.51 and an M_n of 11.2 kg/mol (Fig. S1, Table S1), close to that calculated by ^{1}H NMR. No free thiol was present in the PEG–PDTC

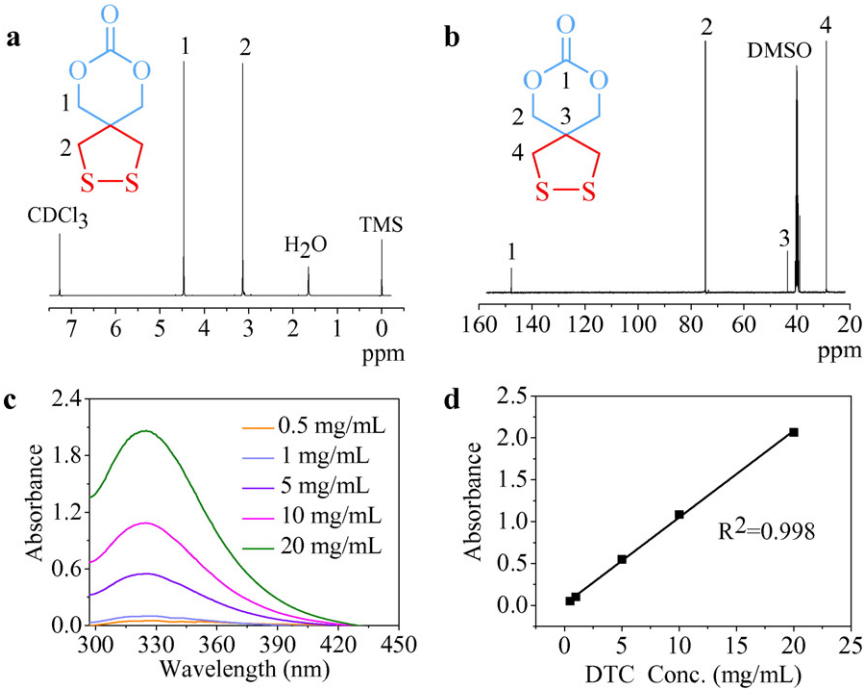

Fig. 1. Characterizations of DTC. (a) ^{1}H NMR spectrum (400 MHz, $CDCl_3$) of DTC. (b) ^{13}C NMR spectrum (100 MHz, DMSO-d_6) of DTC. (c) UV spectrum of DTC in DMF at concentrations ranging from 0.5 to 20 mg/mL. (d) Correlation between DTC concentration and UV absorbance at 330 nm.

block copolymer as revealed by Ellman's test. Moreover, UV spectrum displayed a strong absorbance of a dithiolane ring at 330 nm, comparable to that of the DTC monomer at the same concentration, corroborating that dithiolane groups are intact during polymerization and workup procedure.

3.2. Micelle formation and controlled drug release

PEG-*b*-PDTC diblock copolymer self-assembled into robust micellar nanoparticles with a diameter of *ca.* 150 nm and a polydispersity index (PDI) of 0.18, as shown by dynamic light scattering (DLS) and transmission electron microscopy (TEM) measurements (Fig. 3a). Interestingly, the UV spectrum of micelle dispersions after workup procedure showed a complete disappearance of the absorbance at 330 nm (Fig. 3b), indicating that the dithiolane rings in the micellar core undergo automatic ring-opening polymerization to form linear polydisulfide, similar to lipoic acid nanoparticles following treatment with catalytic dithiothreitol [30–31]. In accordance, SCID-Ms exhibited superior colloidal stability against 10% serum and extensive dilution (Fig. S2a), while quickly swelling to *ca.* 338 nm in 4 h and 724 nm in 12 h in response to 10 mM glutathione (GSH, mimicking the reductive environment in the cytoplasm) (Fig. S2b), indicating that micellar nanoparticles are de-crosslinked and destabilized by GSH through cleavage of disulfide crosslinks into two hydrophilic thiol groups. Zeta potential measurements showed that SCID-Ms had a neutral surface charge.

We selected DOX, a potent clinical chemotherapeutics, to assess the drug loading and delivery behaviors of SCID-Ms. Notably, DOX could efficiently be loaded into SCID-Ms with a high drug loading content (DLC)

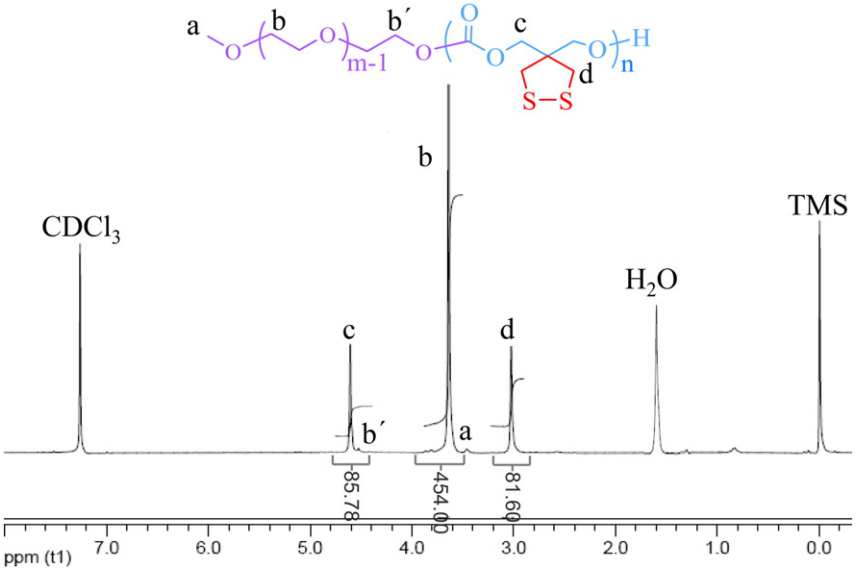

Fig. 2. ^{1}H NMR spectrum (400 MHz, $CDCl_3$) of PEG-*b*-PDTC diblock copolymer.

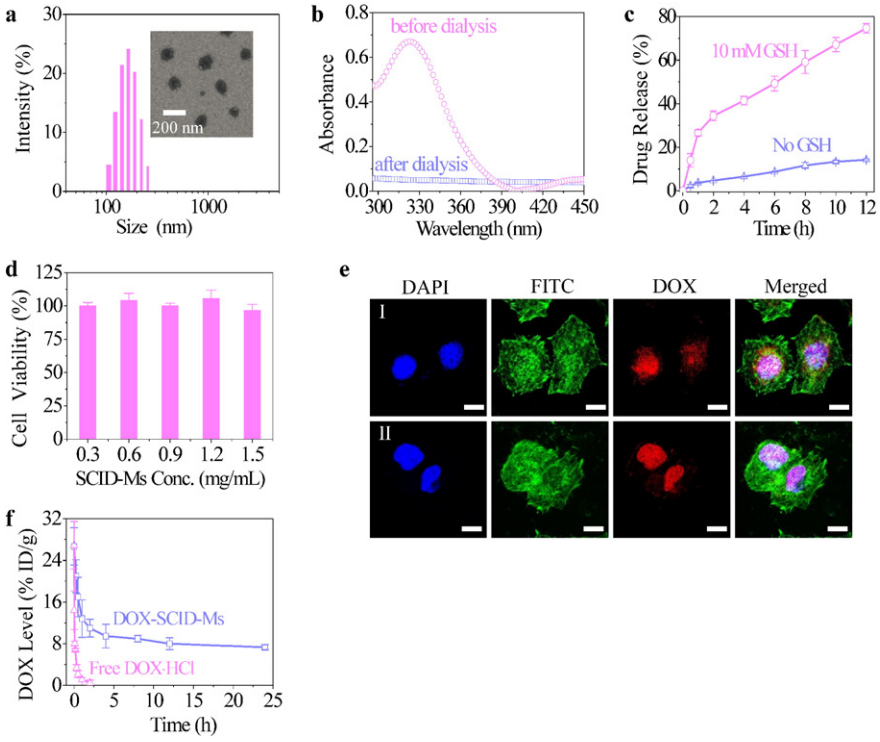

Fig. 3. (a) DLS and TEM profiles of SCID-Ms. (b) UV spectra of PEG-*b*-PDTC micellar nanoparticles before and after workup. (c) *In vitro* drug release behaviors of DOX-SCID-Ms. The release studies were performed at pH 7.4 and 37 °C either in the presence or absence of 10 mM GSH. (d) MTT assays of blank SCID-Ms in B16 melanoma cells. (e) CLSM images of B16 melanoma cells following 2 h incubation with DOX-SCID-Ms (I) and free DOX·HCl (II). DOX dosage was 10.0 μg/mL. For each panel, the images from left to right show cell nuclei stained by DAPI (blue), cytoskeleton stained by phalloidin-FITC (green), DOX fluorescence in cells (red), and overlays of the three images. The scale bars correspond to 20 μm. (f) *In vivo* pharmacokinetics of DOX-SCID-Ms and free DOX·HCl in C57BL/6 mice.

of 14.4 wt.% (Table S2). The *in vitro* release studies revealed a low DOX release from SCID-Ms (less than 15% in 12 h) under physiological conditions (pH 7.4 and 37 °C) (Fig. 3c). In contrast, 75% DOX was released in 12 h in the presence of 10 mM GSH under otherwise identical conditions, likely due to fast de-crosslinking and swelling of micellar core. It appears that SCID-Ms provide a unique solution to simultaneously resolve the drug leakage and slow intracellular drug release problems confronted by common biodegradable micellar nanoparticles.

As revealed by MTT assays, SCID-Ms were non-toxic to B16 cells up to a tested concentration of 1.5 mg/mL (Fig. 3d), confirming their good biocompatibility. DOX-SCID-Ms displayed, as expected, a significant anti-tumor effect towards B16 cells with a half-maximal inhibitory concentration (IC_{50}) of 2.98 μg DOX equiv./mL (**Fig. S3**). The somewhat higher IC_{50} observed for DOX-SCID-Ms as compared to free DOX·HCl is likely due to the inhibited cell uptake by the PEG stealth effect. CLSM observed strong DOX fluorescence in the nuclei of B16 cells following 2 h incubation with DOX-SCID-Ms, approaching those with free DOX (Fig. 3e), confirming fast de-crosslinking of DOX-SCID-Ms and efficient cytoplasmic DOX release.

3.3. In vivo pharmacokinetics, biodistribution and tolerability of DOX-SCID-Ms

The *in vivo* pharmacokinetic studies in C57BL/6 mice showed that DOX-SCID-Ms had a prolonged circulation time with an elimination phase half-life ($t_{1/2,\beta}$) of 5.40 h and an area under the curve (AUC) of 56.2 μg/mL h (Fig. 3f), which were *ca.* 20 times higher than those of free DOX·HCl. Notably, paclitaxel-loaded core-crosslinked polymeric micelles did not show much improvement in the pharmacokinetics [45]. The significantly improved pharmacokinetics for DOX-SCID-Ms is likely due to their much higher crosslinking density that results in not only superior stability but also inhibited drug leakage *in vivo*. The *in vivo* biodistribution studies in B16 melanoma-bearing C57BL/6 mice showed that DOX-SCID-Ms significantly enhanced DOX accumulation in the tumor, reaching 3.13% of injected dose per gram of tissue (%ID/g) at 6 h post injection (Fig. 4a). Moreover, the DOX level in the tumor remained high at 24 h post injection of DOX-SCID-Ms, in sharp contrast to the quickly diminishing DOX concentration observed in mice treated with free DOX·HCl. Noteworthy, the tumor-to-normal tissue ratio (T/N) data showed that DOX-SCID-Ms caused 5–15 fold enhancement of tumor selectivity as compared to free DOX·HCl (Fig. S4).

The maximum-tolerated dose (MTD) studies displayed that *i.v.* injection of DOX-SCID-Ms at a single dose of 50 or 100 mg DOX equiv./kg induced little body weight loss of C57BL/6 mice in 10 days (Fig. 4b), indicating that DOX-SCID-Ms have an MTD value of over 100 mg DOX equiv./kg. In sharp contrast, more than 18% body weight loss was observed for mice treated with 10 mg DOX/kg of free DOX·HCl. DOX-SCID-Ms with at least 10-fold enhancement of MTD as compared to free DOX·HCl possess, to the best of our knowledge, the highest MTD among the reported nanoparticulate formulations. For instance, chimaeric polypeptide–doxorubicin conjugate nanoparticles showed a 4-fold higher MTD than free drug [46]. An MTD of 15 mg/kg was reported for squalenoyl doxorubicin (SQ-Dox) [47]. This unprecedented MTD and thereby significantly increased therapeutic window of DOX is most likely attributed to their extraordinary stability and prohibited premature drug release as a result of dense core-crosslinking. The clinical applications of many drugs including DOX are dose limited due to a narrow therapeutic window.

3.4. In vivo treatment of B16 melanoma-bearing C57BL/6 mice by DOX-SCID-Ms

We evaluated the therapeutic effects of DOX-SCID-Ms using malignant B16 melanoma-bearing C57BL/6 mice. The results showed that

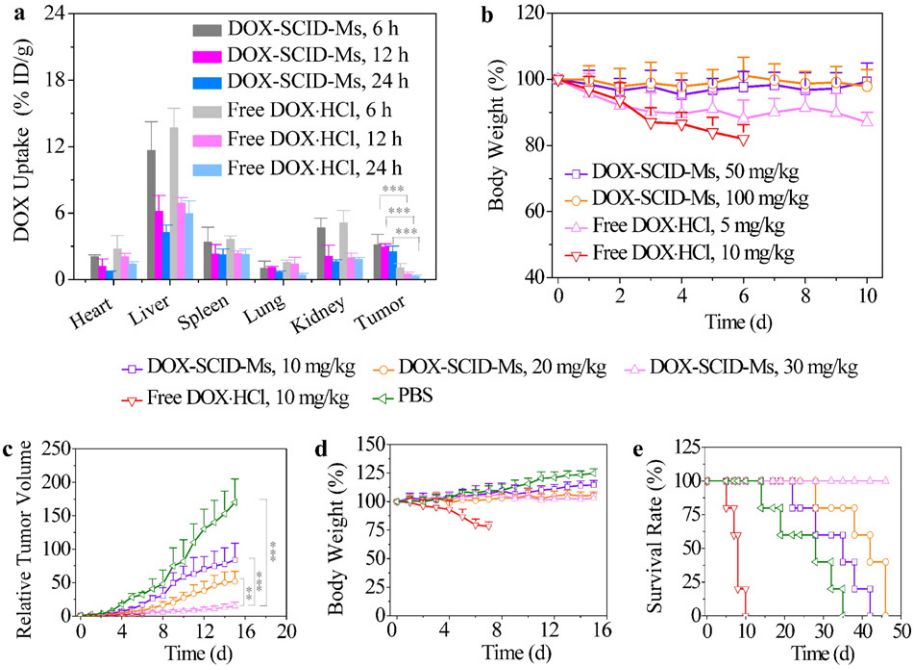

Fig. 4. *In vivo* biodistribution and therapeutic effects of DOX-SCID-Ms in B16 melanoma-bearing C57BL/6 mice. (a) *In vivo* biodistribution of DOX-SCID-Ms. DOX levels in different organs and tumor, expressed as percentage of injected dose per gram of tissue (%ID/g), were determined using fluorescence spectroscopy. Free DOX·HCl was used as a control. Data are presented as mean ± SD ($n = 5$). (b) MTD studies of DOX-SCID-Ms in tumor-free C57BL/6 mice (n = 5). (c) Tumor growth suppression with DOX-SCID-Ms. The drug was given on days 0, 2, 4, 6 and 8. Data are presented as mean ± SD ($n = 6$). $^{**}p < 0.01$, $^{***}p < 0.001$ (Student's *t*-test). (d) Body weight change of tumor-bearing mice in time. Data are presented as mean ± SD ($n = 6$). (e) Survival rates of tumor-bearing mice following different treatments.

DOX-SCID-Ms inhibited tumor growth in a dose-dependent manner, in which tumor progression was significantly suppressed at a dosage of 30 mg DOX equiv./kg (Fig. 4c). Though free DOX·HCl inhibited tumor growth at 10 mg/kg, it also led to *ca.* 22% body weight loss in 7 days (Fig. 4d). In comparison, little body weight change was observed for the mice treated with DOX-SCID-Ms, indicating that DOX-SCID-Ms cause little systemic toxicity. Remarkably, mice treated with 30 mg DOX equiv./kg DOX-SCID-Ms showed a 100% survival rate in an experimental period of 46 days (Fig. 4e). The histological analyses using H&E staining revealed that DOX-SCID-Ms at 30 mg DOX equiv./kg caused little damage to the major organs including the heart, liver and kidney, while heart tissue of mice treated with free DOX·HCl showed apparent atrophy cardiac myocytes and infiltration of inflammatory cells (Fig. S5), supporting that DOX-SCID-Ms have low systemic toxicity.

3.5. Fabrication and in vitro assessments of cRGD-installed DOX-SCID-Ms

To achieve active tumor targeting ability, we further decorated SCID-Ms with a cRGD peptide, which displays a high selectivity towards $\alpha_v\beta_3$ integrin-overexpressing angiogenic endothelial cells as well as several malignant tumor cells such as B16 melanoma cells and human U87 glioma cells *in vitro* and *in vivo* [47–50]. cRGD-PEG-*b*-PDTC was readily prepared with an M_n of 6.5–3.7 kg/mol, as calculated by ^{1}H NMR, through ring-opening polymerization of DTC using NHS-PEG-OH (M_n = 6.5 kg/mol) as an initiator followed by reacting with cRGDfK (Scheme S1). cRGD-functionalized SCID-Ms (cRGD/SCID-Ms) were prepared with varying cRGD densities by co-self-assembly of cRGD-PEG-*b*-PDTC and PEG-*b*-PDTC copolymers. Notably, cRGD-PEG-*b*-PDTC was designed to contain a longer PEG than PEG-*b*-PDTC (6.5 *versus* 5.0 kg/mol) in order to fully expose cRGD ligands at the micelle surface for optimal tumor targeting effect. DLS measurements displayed that cRGD/SCID-Ms had a hydrodynamic size of 150–155 nm, similar to that of the non-targeting SCID-Ms. Moreover, cRGD/SCID-Ms as SCID-Ms had a neutral surface charge. The blank cRGD/SCID-Ms, similar to SCID-Ms, were non-cytotoxic at a micelle concentration of 1.0 mg/mL (Fig. S6a).

To study their active targetability, B16 cells were incubated with cRGD/DOX-SCID-Ms for 4 h, the media were removed and replenished with fresh culture media, and the cells were cultured for another 44 h. MTT assays revealed that the antitumor effect of DOX-loaded cRGD/SCID-Ms (cRGD/DOX-SCID-Ms) to B16 cells intimately depended on cRGD contents, in which IC_{50} decreased almost linearly with increasing cRGD densities from 0 to 20% (Fig. S6b). Interestingly, cRGD20/DOX-SCID-Ms revealed a low IC_{50} of 2.02 μg DOX equiv./mL, which was significantly lower than 12.51 μg DOX equiv./mL for commercial pegylated liposomal DOX (DOX-LPs) control. DOX-LPs are one of the very few nanomedicines widely used in the clinics for the treatment of various cancers [51]. It is interesting to note that further increasing cRGD density to 30% resulted in only a slight decrease of IC_{50}. Flow cytometric analyses showed that cellular DOX level in B16 cells following 4 h incubation with cRGD/DOX-SCID-Ms increased with increasing cRGD densities from 0 to 20% and almost levelled off at cRGD density to 30% (Fig. S7), in accordance with the MTT results. In the following, we selected cRGD20/SCID-Ms for further studies. CLSM results showed very strong DOX fluorescence in the cell nuclei following 8 h incubation with cRGD20/DOX-SCID-Ms, which was much higher than that in DOX-LPs or DOX-SCID-Ms treated cells as well as in cells pre-treated with free cRGD prior to adding cRGD20/DOX-SCID-Ms (Fig. S8). These observations support that cRGD/DOX-SCID-Ms are taken up by B16 cells *via* the receptor-mediated endocytosis mechanism.

3.6. In vivo pharmacokinetics and biodistribution of cRGD-directed DOX-SCID-Ms

The *in vivo* pharmacokinetic results demonstrated that cRGD20/DOX-SCID-Ms had a long circulation time with a $t_{1/2\beta}$ of 6.19 h and an AUC of 62.0 μg/mL h, comparable to DOX-LPs (Fig. 5a). cRGD20/DOX-SCID-Ms exhibited a slightly longer circulation time than DOX-SCID-Ms, which is likely due to their longer PEG chain, indicating that surface decoration with a 20% cRGD peptide has no negative effect to the *in vivo* pharmacokinetics of the micellar nanoparticles. The biodistribution studies revealed that tumor accumulation of cRGD20/DOX-SCID-Ms

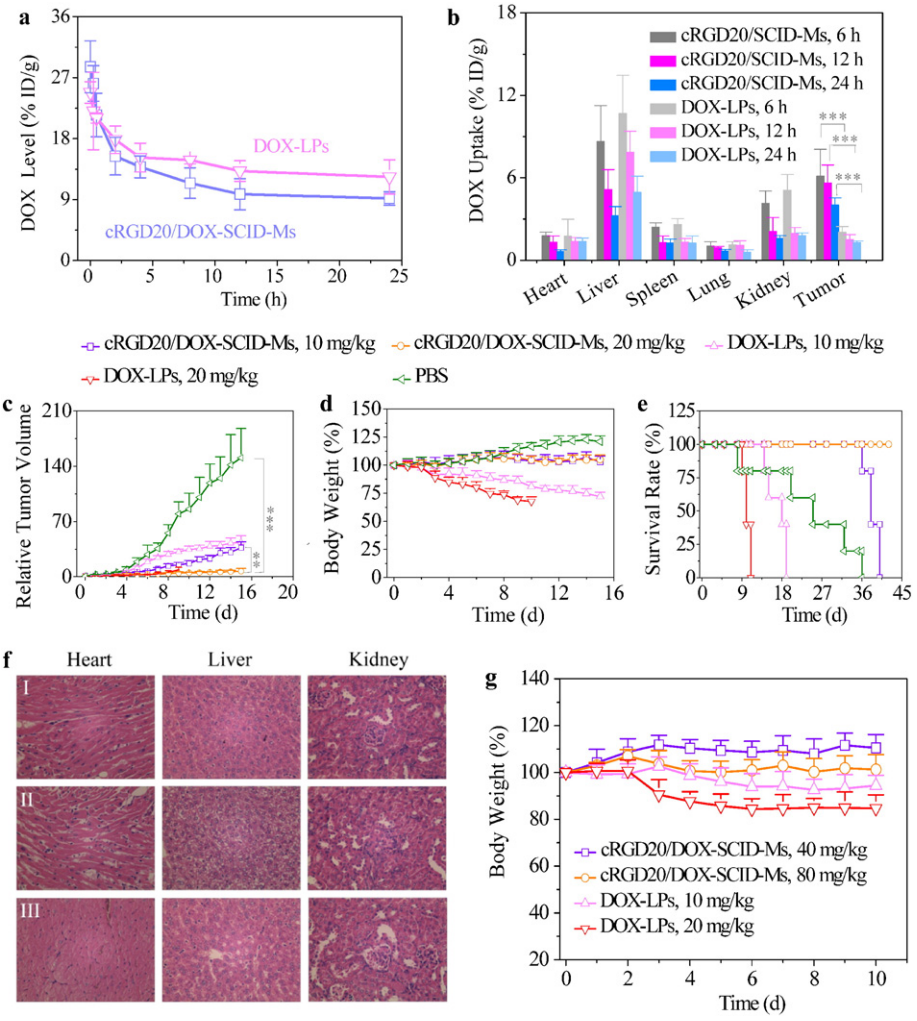

Fig. 5. *In vivo* therapeutic effects of cRGD20/DOX-SCID-Ms in $\alpha_v\beta_3$ overexpressing B16 melanoma-bearing C57BL/6 mice. (a) *In vivo* pharmacokinetics of cRGD20/DOX-SCID-Ms and DOX-LPs in C57BL/6 mice. (b) *In vivo* biodistribution of cRGD20/DOX-SCID-Ms and DOX-LPs. Data are presented as mean ± SD ($n = 5$). (c) Tumor growth suppression with cRGD20/DOX-SCID-Ms and DOX-LPs. The drug was given on days 0, 2, 4, 6 and 8. Data are presented as mean ± SD ($n = 6$). (d) Body weight change of tumor-bearing mice following different treatments in time. Data are presented as mean ± SD ($n = 6$). (e) Survival rates of tumor-bearing mice ($n = 5$). (f) Histological analyses of the heart, liver and kidney of mice following treatment with 20 mg/kg cRGD20/DOX-SCID-Ms (I), 10 mg/kg DOX-LPs (II), and PBS (III). (g) MTD studies of cRGD20/DOX-SCID-Ms in tumor-free C57BL/6 mice ($n = 5$). $^{**}p < 0.01$, $^{***}p < 0.001$ (Student's *t*-test).

was as high as 6.13% ID/g at 6 h post injection, which was *ca.* 3-fold higher than that for DOX-LPs (Fig. 5b). Notably, significant tumor accumulation was also observed for cRGD20/DOX-SCID-Ms at 24 h after injection, confirming that cRGD functionalization of nanoparticles can markedly enhance their tumor accumulation and retention [52–53]. The plot of T/N ratios reveals that cRGD20/DOX-SCID-Ms resulted in 3–7 fold better tumor selectivity than DOX-LPs (Fig. S9).

3.7. Targeted treatment of B16 melanoma-bearing mice by cRGD-directed DOX-SCID-Ms

The *in vivo* targetability and treatment effects of cRGD20/DOX-SCID-Ms were studied in B16 melanoma-bearing C57BL/6 mice and compared with DOX-LPs. The results showed that cRGD20/DOX-SCID-Ms effectively inhibited tumor growth at 20 mg DOX equiv./kg (Fig. 5c). The installment of cRGD on the surface of DOX-SCID-Ms significantly enhanced their anti-tumor efficacy (Fig. S10). Importantly, mice treated with cRGD20/DOX-SCID-Ms had little change in body weight (Fig. 5d), indicating that they cause little side effects. In contrast, DOX-LPs induced significant body weight loss at dosages of 10 and 20 mg DOX equiv./kg. Notably, mice treated with cRGD20/DOX-SCID-Ms exhibited markedly improved survival rate over those with DOX-LPs (Fig. 5e). In particular, 100% survival rate was observed in an experimental period of 43 days at 20 mg DOX equiv./kg. As revealed by the histological analyses, cRGD20/DOX-SCID-Ms caused little damage at 20 mg DOX equiv./kg to the normal organs like the heart, liver and kidney (Fig. 5f). In contrast, DOX-LPs also led to hepatotoxicity and renal toxicity besides the obvious hand–foot syndrome. Fig. 5g shows that cRGD20/DOX-SCID-Ms possessed a superior MTD of over 80 mg DOX equiv./kg, which was at least 4-fold higher than DOX-LPs. This remarkable tolerance of cRGD20/DOX-SCID-M offers a viable treatment window to achieving extraordinary efficacy while maintaining a low systemic toxicity.

4. Conclusions

We have designed and developed self-crosslinkable and intracellularly decrosslinkable biodegradable micellar nanoparticles (SCID-Ms) for high-efficiency targeted cancer chemotherapy *in vivo*. Notably, nanotherapeutics based on SCID-Ms bear all desired functions in one including high drug loading, superior stability, long-circulation time, minimal drug leakage, triggered drug release inside the tumor cells, and high tolerated dose. DOX-loaded SCID-Ms can effectively inhibit tumor

growth and improve the survival rate of malignant B16 melanoma-bearing C57BL/6 mice while causing little systemic toxicity at a dosage of 30 mg DOX equiv./kg. We have further demonstrated that SCID-Ms can be readily functionalized with tumor-homing cRGD peptide. Remarkably, the *in vivo* results in $\alpha_v\beta_3$ overexpressing B16 melanoma-bearing mice clearly show that cRGD-directed micellar doxorubicin brings about markedly enhanced tumor accumulation and selectivity, significantly improved therapeutic efficacy, and largely reduced side effects as compared to clinically used pegylated liposomal doxorubicin (DOX-LPs). It is important to note that nanotherapeutics based on SCID-Ms are simple and easy to prepare in a large scale. Moreover, the physiochemical properties of SCID-Ms can be tailored by copolymerizing with common cyclic esters and carbonates such as D,L-lactide and trimethylene carbonate for efficient loading and delivery of various chemotherapeutic agents. SCID-Ms with great simplicity, multifunctionality and safety have a tremendous potential for translational nanomedicine research.

Acknowledgements

This work is supported by research grants from the National Natural Science Foundation of China (NSFC 51273139, 51473111 and 51561135010) and the National Science Fund for Distinguished Young Scholars (NSFC 51225302). Z.Z. thanks the Friedrich Wilhelm Bessel Research Award from the Alexander von Humboldt Foundation.

Appendix A. Supplementary

Supplementary data to this article can be found online at http://dx.doi.org/10.1016/j.jconrel.2016.05.060.

References

[1] D. Peer, J.M. Karp, S. Hong, O.C. Farokhzad, R. Margalit, R. Langer, Nanocarriers as an emerging platform for cancer therapy, Nat. Nanotechnol. 2 (2007) 751–760.
[2] C.J. Cheng, G.T. Tietjen, J.K. Saucier-Sawyer, W.M. Saltzman, A holistic approach to targeting disease with polymeric nanoparticles, Nat. Rev. Drug Discov. 14 (2015) 239–247.
[3] G. Gaucher, R.H. Marchessault, J.-C. Leroux, Polyester-based micelles and nanoparticles for the parenteral delivery of taxanes, J. Control. Release 143 (2010) 2–12.
[4] N. Bertrand, J. Wu, X. Xu, N. Kamaly, O.C. Farokhzad, Cancer nanotechnology: the impact of passive and active targeting in the era of modern cancer biology, Adv. Drug Deliv. Rev. 66 (2014) 2–25.
[5] V.P. Chauhan, R.K. Jain, Strategies for advancing cancer nanomedicine, Nat. Mater. 12 (2013) 958–962.
[6] C. Deng, Y. Jiang, R. Cheng, F. Meng, Z. Zhong, Biodegradable polymeric micelles for targeted and controlled anticancer drug delivery: promises, progress and prospects, Nano Today 7 (2012) 467–480.
[7] S.C. Owen, D.P. Chan, M.S. Shoichet, Polymeric micelle stability, Nano Today 7 (2012) 53–65.
[8] C.F. van Nostrum, Covalently cross-linked amphiphilic block copolymer micelles, Soft Matter 7 (2011) 3246–3259.
[9] S. Mura, J. Nicolas, P. Couvreur, Stimuli-responsive nanocarriers for drug delivery, Nat. Mater. 12 (2013) 991–1003.
[10] V.P. Torchilin, Multifunctional, stimuli-sensitive nanoparticulate systems for drug delivery, Nat. Rev. Drug Discov. 13 (2014) 813–827.
[11] Z. Ge, S. Liu, Functional block copolymer assemblies responsive to tumor and intracellular microenvironments for site-specific drug delivery and enhanced imaging performance, Chem. Soc. Rev. 42 (2013) 7289–7325.
[12] E. Fleige, M.A. Quadir, R. Haag, Stimuli-responsive polymeric nanocarriers for the controlled transport of active compounds: concepts and applications, Adv. Drug Deliv. Rev. 64 (2012) 866–884.
[13] R. Cheng, F. Meng, C. Deng, Z. Zhong, Bioresponsive polymeric nanotherapeutics for targeted cancer chemotherapy, Nano Today 10 (2015) 656–670.
[14] K. Raemdonck, S.C. De Smedt, Lessons in simplicity that should shape the future of drug delivery, Nat. Biotechnol. 33 (2015) 1026–1027.
[15] V.J. Venditto, F.C. Szoka, Cancer nanomedicines: so many papers and so few drugs! Adv. Drug Deliv. Rev. 65 (2013) 80–88.
[16] A.S. Hoffman, Stimuli-responsive polymers: biomedical applications and challenges for clinical translation, Adv. Drug Deliv. Rev. 65 (2013) 10–16.
[17] C.M. Dawidczyk, C. Kim, J.H. Park, L.M. Russell, K.H. Lee, M.G. Pomper, P.C. Searson, State-of-the-art in design rules for drug delivery platforms: lessons learned from FDA-approved nanomedicines, J. Control. Release 187 (2014) 133–144.
[18] S. Eetezadi, S.N. Ekdawi, C. Allen, The challenges facing block copolymer micelles for cancer therapy: in vivo barriers and clinical translation, Adv. Drug Deliv. Rev. 91 (2015) 7–22.
[19] Y. Min, J.M. Caster, M.J. Eblan, A.Z. Wang, Clinical translation of nanomedicine, Chem. Rev. 115 (2015) 11147–11190.
[20] T. Lammers, W. Hennink, G. Storm, Tumour-targeted nanomedicines: principles and practice, Br. J. Cancer 99 (2008) 392–397.
[21] H. Cabral, K. Kataoka, Progress of drug-loaded polymeric micelles into clinical studies, J. Control. Release 190 (2014) 465–476.
[22] A. Gabizon, M. Bradbury, U. Prabhakar, W. Zamboni, S. Libutti, P. Grodzinski, Cancer nanomedicines: closing the translational gap, Lancet 384 (2014) 2175–2176.
[23] L.S. Nair, C.T. Laurencin, Biodegradable polymers as biomaterials, Prog. Polym. Sci. 32 (2007) 762–798.
[24] F. Suriano, R. Pratt, J.P. Tan, N. Wiradharma, A. Nelson, Y.-Y. Yang, P. Dubois, J.L. Hedrick, Synthesis of a family of amphiphilic glycopolymers via controlled ring-opening polymerization of functionalized cyclic carbonates and their application in drug delivery, Biomaterials 31 (2010) 2637–2645.
[25] W. Chen, F. Meng, R. Cheng, C. Deng, J. Feijen, Z. Zhong, Advanced drug and gene delivery systems based on functional biodegradable polycarbonates and copolymers, J. Control. Release 190 (2014) 398–414.
[26] J. Feng, R.-X. Zhuo, X.-Z. Zhang, Construction of functional aliphatic polycarbonates for biomedical applications, Prog. Polym. Sci. 37 (2012) 211–236.
[27] K. Fukushima, Poly (trimethylene carbonate)-based polymers engineered for biodegradable functional biomaterials, Biomater. Sci. 4 (2016) 9–24.
[28] S. Schüller-Ravoo, E. Zant, J. Feijen, D.W. Grijpma, Preparation of a designed poly (trimethylene carbonate) microvascular network by stereolithography, Adv. Healthcare Mater. 3 (2014) 2004–2011.
[29] U. Singh, I. Jialal, Retracted: alpha-lipoic acid supplementation and diabetes, Nutr. Rev. 66 (2008) 646–657.
[30] Y.L. Li, L. Zhu, Z. Liu, R. Cheng, F. Meng, J.H. Cui, S.J. Ji, Z. Zhong, Reversibly stabilized multifunctional dextran nanoparticles efficiently deliver doxorubicin into the nuclei of cancer cells, Angew. Chem. Int. Ed. 48 (2009) 9914–9918.
[31] Y. Zhong, J. Zhang, R. Cheng, C. Deng, F. Meng, F. Xie, Z. Zhong, Reversibly crosslinked hyaluronic acid nanoparticles for active targeting and intelligent delivery of doxorubicin to drug resistant CD44+ human breast tumor xenografts, J. Control. Release 205 (2015) 144–154.
[32] J. Wu, L. Zhao, X. Xu, N. Bertrand, W.I. Choi, B. Yameen, J. Shi, V. Shah, M. Mulvale, J.L. MacLean, Hydrophobic cysteine poly (disulfide)-based redox-hypersensitive nanoparticle platform for cancer theranostics, Angew. Chem. Int. Ed. 127 (2015) 9350–9355.
[33] R. Cheng, F. Feng, F. Meng, C. Deng, J. Feijen, Z. Zhong, Glutathione-responsive nanovehicles as a promising platform for targeted intracellular drug and gene delivery, J. Control. Release 152 (2011) 2–12.
[34] J. Li, M. Huo, J. Wang, J. Zhou, J.M. Mohammad, Y. Zhang, Q. Zhu, A.Y. Waddad, Q. Zhang, Redox-sensitive micelles self-assembled from amphiphilic hyaluronic acid-deoxycholic acid conjugates for targeted intracellular delivery of paclitaxel, Biomaterials 33 (2012) 2310–2320.
[35] Y.-C. Wang, F. Wang, T.-M. Sun, J. Wang, Redox-responsive nanoparticles from the single disulfide bond-bridged block copolymer as drug carriers for overcoming multidrug resistance in cancer cells, Bioconjug. Chem. 22 (2011) 1939–1945.
[36] M. Huo, J. Yuan, L. Tao, Y. Wei, Redox-responsive polymers for drug delivery: from molecular design to applications, Polym. Chem. 5 (2014) 1519–1528.
[37] M. Zhao, A. Biswas, B. Hu, K.-I. Joo, P. Wang, Z. Gu, Y. Tang, Redox-responsive nanocapsules for intracellular protein delivery, Biomaterials 32 (2011) 5223–5230.
[38] S.S. Dunn, S. Tian, S. Blake, J. Wang, A.L. Galloway, A. Murphy, P.D. Pohlhaus, J.P. Rolland, M.E. Napier, J.M. DeSimone, Reductively responsive siRNA-conjugated hydrogel nanoparticles for gene silencing, J. Am. Chem. Soc. 134 (2012) 7423–7430.
[39] W. Chen, K. Achazi, B. Schade, R. Haag, Charge-conversional and reduction-sensitive poly (vinyl alcohol) nanogels for enhanced cell uptake and efficient intracellular doxorubicin release, J. Control. Release 205 (2015) 15–24.
[40] P.M. Klein, K. Müller, C. Gutmann, P. Kos, A.K. Levacic, D. Edinger, M. Höhn, J.-C. Leroux, M.A. Gauthier, E. Wagner, Twin disulfides as opportunity for improving stability and transfection efficiency of oligoaminoethane polyplexes, J. Control. Release 205 (2015) 109–119.
[41] L. Brülisauer, M.A. Gauthier, J.-C. Leroux, Disulfide-containing parenteral delivery systems and their redox-biological fate, J. Control. Release 195 (2014) 147–154.
[42] G. Saito, J.A. Swanson, K.-D. Lee, Drug delivery strategy utilizing conjugation via reversible disulfide linkages: role and site of cellular reducing activities, Adv. Drug Deliv. Rev. 55 (2003) 199–215.
[43] F. Meng, W.E. Hennink, Z. Zhong, Reduction-sensitive polymers and bioconjugates for biomedical applications, Biomaterials 30 (2009) 2180–2198.
[44] M. Balakirev, G. Schoehn, J. Chroboczek, Lipoic acid-derived amphiphiles for redox-controlled DNA delivery, Chem. Biol. 7 (2000) 813–819.
[45] M. Talelli, M. Barz, C.J. Rijcken, F. Kiessling, W.E. Hennink, T. Lammers, Core-crosslinked polymeric micelles: principles, preparation, biomedical applications and clinical translation, Nano Today 10 (2015) 93–117.
[46] J.A. MacKay, M. Chen, J.R. McDaniel, W. Liu, A.J. Simnick, A. Chilkoti, Self-assembling chimeric polypeptide–doxorubicin conjugate nanoparticles that abolish tumours after a single injection, Nat. Mater. 8 (2009) 993–999.
[47] F. Danhier, A.L. Breton, V.r. Préat, RGD-based strategies to target alpha (v) beta (3) integrin in cancer therapy and diagnosis, Mol. Pharm. 9 (2012) 2961–2973.
[48] N. Nasongkla, X. Shuai, H. Ai, B.D. Weinberg, J. Pink, D.A. Boothman, J. Gao, cRGD-functionalized polymer micelles for targeted doxorubicin delivery, Angew. Chem. Int. Ed. 116 (2004) 6483–6487.
[49] S. Kunjachan, R. Pola, F. Gremse, B. Theek, J. Ehling, D. Moeckel, B. Hermanns-Sachweh, M. Pechar, K. Ulbrich, W.E. Hennink, Passive versus active tumor targeting

using RGD- and NGR-modified polymeric nanomedicines, Nano Lett. 14 (2014) 972–981.
[50] Y. Zhong, F. Meng, C. Deng, Z. Zhong, Ligand-directed active tumor-targeting polymeric nanoparticles for cancer chemotherapy, Biomacromolecules 15 (2014) 1955–1969.
[51] Y.C. Barenholz, Doxil®—the first FDA-approved nano-drug: lessons learned, J. Control. Release 160 (2012) 117–134.
[52] Y. Miura, T. Takenaka, K. Toh, S. Wu, H. Nishihara, M.R. Kano, Y. Ino, T. Nomoto, Y. Matsumoto, H. Koyama, Cyclic RGD-linked polymeric micelles for targeted delivery of platinum anticancer drugs to glioblastoma through the blood–brain tumor barrier, ACS Nano 7 (2013) 8583–8592.
[53] M. Benezra, O. Penate-Medina, P.B. Zanzonico, D. Schaer, H. Ow, A. Burns, E. DeStanchina, V. Longo, E. Herz, S. Iyer, Multimodal silica nanoparticles are effective cancer-targeted probes in a model of human melanoma, J. Clin. Invest. 121 (2011) 2768–2780.